Eur. Phys. J. C 34, 109–125 (2004)
Digital Object Identifier (DOI) 10.1140/epjc/s2004-01708-6

THE EUROPEAN PHYSICAL JOURNAL C

Measurement of the forward-backward asymmetries of $e^+e^- \to Z \to b\bar{b}$ and $e^+e^- \to Z \to c\bar{c}$ using prompt leptons

The DELPHI Collaboration

J. Abdallah[25], P. Abreu[22], W. Adam[51], P. Adzic[11], T. Albrecht[17], T. Alderweireld[2], R. Alemany-Fernandez[8], T. Allmendinger[17], P. Allport[23], U. Amaldi[29], N. Amapane[45], S. Amato[48], E. Anashkin[36], A. Andreazza[28], S. Andringa[22], N. Anjos[22], P. Antilogus[25], W-D. Apel[17], Y. Arnoud[14], S. Ask[26], B. Asman[44], E. Augustin[25], A. Augustinus[8], P. Baillon[8], A. Ballestrero[46], P. Bambade[20], R. Barbier[27], D. Bardin[16], G. Barker[17], A. Baroncelli[39], M. Battaglia[8], M. Baubillier[25], K.-H. Becks[53], M. Begalli[6], A. Behrmann[53], E. Ben-Haim[20], N. Benekos[32], A. Benvenuti[5], C. Berat[14], M. Berggren[25], L. Berntzon[44], D. Bertrand[2], M. Besancon[40], N. Besson[40], D. Bloch[9], M. Blom[31], M. Bluj[52], M. Bonesini[29], M. Boonekamp[40], L. Booth[23], G. Borisov[21], O. Botner[49], B. Bouquet[20], V. Bowcock[23], I. Boyko[16], M. Bracko[43], R. Brenner[49], E. Brodet[35], P. Bruckman[18], M. Brunet[7], L. Bugge[33], P. Buschmann[53], M. Calvi[29], T. Camporesi[8], V. Canale[38], F. Carena[8], N. Castro[22], F. Cavallo[5], M. Chapkin[42], Ph. Charpentier[8], P. Checchia[36], R. Chierici[8], P. Chliapnikov[42], J. Chudoba[8], U. Chung[8], K. Cieslik[18], P. Collins[8], R. Contri[13], G. Cosme[20], F. Cossutti[47], J. Costa[50], D. Crennell[37], J. Cuevas[34], J. D'Hondt[2], J. Dalmau[44], T. da Silva[48], W. Da Silva[25], G. Della Ricca[47], A. De Angelis[47], W. De Boer[17], C. De Clercq[2], B. De Lotto[47], N. De Maria[45], A. De Min[36], L. de Paula[48], L. Di Ciaccio[38], A. Di Simone[39], K. Doroba[52], J. Drees[53,8], M. Dris[32], G. Eigen[4], T. Ekelof[49], M. Ellert[49], M. Elsing[8], C. Espirito Santo[22], G. Fanourakis[11], D. Fassouliotis[11,3], M. Feindt[17], J. Fernandez[41], A. Ferrer[50], F. Ferro[13], U. Flagmeyer[53], H. Foeth[8], E. Fokitis[32], F. Fulda-Quenzer[20], J. Fuster[50], M. Gandelman[48], C. Garcia[50], Ph. Gavillet[8], E. Gazis[32], R. Gokieli[8,52], B. Golob[43], G. Gomez-Ceballos[41], P. Goncalves[22], E. Graziani[39], G. Grosdidier[20], K. Grzelak[52], J. Guy[37], C. Haag[17], A. Hallgren[49], K. Hamacher[53], K. Hamilton[35], S. Haug[33], F. Hauler[17], V. Hedberg[26], M. Hennecke[17], H. Herr[8], J. Hoffman[52], S-O. Holmgren[44], J. Holt[8], A. Houlden[23], K. Hultqvist[44], N. Jackson[23], G. Jarlskog[26], P. Jarry[40], D. Jeans[35], K. Johansson[44], D. Johansson[44], P. Jonsson[27], C. Joram[8], L. Jungermann[17], F. Kapusta[25], S. Katsanevas[27], E. Katsoufis[32], G. Kernel[43], P. Kersevan[8,43], U. Kerzel[17], A. Kiiskinen[15], T. King[23], J. Kjaer[8], P. Kluit[31], P. Kokkinias[11], C. Kourkoumelis[3], O. Kouznetsov[16], Z. Krumstein[16], M. Kucharczyk[18], J. Lamsa[1], G. Leder[51], F. Ledroit[14], L. Leinonen[44], R. Leitner[30], J. Lemonne[2], V. Lepeltier[20], T. Lesiak[18], W. Liebig[53], D. Liko[51], A. Lipniacka[44], H. Lopes[48], M. Lopez[34], D. Loukas[11], P. Lutz[40], L. Lyons[35], J. MacNaughton[51], A. Malek[53], S. Maltezos[32], F. Mandl[51], J. Marco[41], R. Marco[41], B. Marechal[48], M. Margoni[36], J-C. Marin[8], C. Mariotti[8], A. Markou[11], C. Martinez-Rivero[41], J. Masik[12], N. Mastroyiannopoulos[11], F. Matorras[41], C. Matteuzzi[29], F. Mazzucato[36], M. Mazzucato[36], R. Mc Nulty[23], C. Meroni[28], E. Migliore[45], W. Mitaroff[51], U. Mjoernmark[26], T. Moa[44], M. Moch[17], K. Moenig[8,10], R. Monge[13], J. Montenegro[31], D. Moraes[48], S. Moreno[22], P. Morettini[13], U. Mueller[53], K. Muenich[53], M. Mulders[31], L. Mundim[6], W. Murray[37], B. Muryn[19], G. Myatt[35], T. Myklebust[33], M. Nassiakou[11], F. Navarria[5], K. Nawrocki[52], R. Nicolaidou[40], M. Nikolenko[16,9], A. Oblakowska-Mucha[19], V. Obraztsov[42], A. Olshevski[16], A. Onofre[22], R. Orava[15], K. Osterberg[15], A. Ouraou[40], A. Oyanguren[50], M. Paganoni[29], S. Paiano[5], P. Palacios[23], H. Palka[18], D. Papadopoulou[32], L. Pape[8], C. Parkes[24], F. Parodi[13], U. Parzefall[8], A. Passeri[39], O. Passon[53], L. Peralta[22], V. Perepelitsa[50], A. Perrotta[5], A. Petrolini[13], J. Piedra[41], L. Pieri[39], F. Pierre[40], M. Pimenta[22], E. Piotto[8], T. Podobnik[43], V. Poireau[8], E. Pol[6], G. Polok[18], P. Poropat[47], V. Pozdniakov[16], N. Pukhaeva[2,16], A. Pullia[29], J. Rames[12], L. Ramler[17], A. Read[33], P. Rebecchi[8], J. Rehn[17], D. Reid[31], R. Reinhardt[53], P. Renton[35], F. Richard[20], J. Ridky[12], M. Rivero[41], D. Rodriguez[41], A. Romero[45], P. Ronchese[36], P. Roudeau[20], T. Rovelli[5], V. Ruhlmann-Kleider[40], D. Ryabtchikov[42], A. Sadovsky[16], L. Salmi[15], J. Salt[50], A. Savoy-Navarro[25], U. Schwickerath[8], A. Segar[35], R. Sekulin[37], M. Siebel[53], A. Sisakian[16], G. Smadja[27], O. Smirnova[26], A. Sokolov[42], A. Sopczak[21], R. Sosnowski[52], T. Spassov[8], M. Stanitzki[17], A. Stocchi[20], J. Strauss[51], B. Stugu[4], M. Szczekowski[52], M. Szeptycka[52], T. Szumlak[19], T. Tabarelli[29], C. Taffard[23], F. Tegenfeldt[49], J. Timmermans[31], L. Tkatchev[16], M. Tobin[23], S. Todorovova[12], B. Tome[22], A. Tonazzo[29], P. Tortosa[50], P. Travnicek[12], D. Treille[8], G. Tristram[7], M. Trochimczuk[52], C. Troncon[28], M-L. Turluer[40], A. Tyapkin[16], P. Tyapkin[16], S. Tzamarias[11], V. Uvarov[42], G. Valenti[5], P. Van Dam[31], J. Van Eldik[8], A. Van Lysebetten[2], N. van Remortel[2], I. Van Vulpen[8], G. Vegni[28], F. Veloso[22], W. Venus[37], P. Verdier[27], V. Verzi[38], D. Vilanova[40], L. Vitale[47], V. Vrba[12], H. Wahlen[53], J. Washbrook[23], C. Weiser[17], D. Wicke[8], J. Wickens[2], G. Wilkinson[35], M. Winter[9], M. Witek[18], O. Yushchenko[42], A. Zalewska[18], P. Zalewski[52], D. Zavrtanik[43], V. Zhuravlov[16], I. Zimin[16], A. Zintchenko[16], M. Zupan[11]

[1] Department of Physics and Astronomy, Iowa State University, Ames IA 50011-3160, USA
[2] Physics Department, Universiteit Antwerpen, Universiteitsplein 1, 2610 Antwerpen, Belgium
and IIHE, ULB-VUB, Pleinlaan 2, 1050 Brussels, Belgium
and Faculté des Sciences, Univ. de l'Etat Mons, Av. Maistriau 19, 7000 Mons, Belgium
[3] Physics Laboratory, University of Athens, Solonos Str. 104, 10680 Athens, Greece
[4] Department of Physics, University of Bergen, Allégaten 55, 5007 Bergen, Norway
[5] Dipartimento di Fisica, Universit à di Bologna and INFN, Via Irnerio 46, 40126 Bologna, Italy
[6] Centro Brasileiro de Pesquisas Físicas, rua Xavier Sigaud 150, 22290 Rio de Janeiro, Brazil
and Depto. de Física, Pont. Univ. Católica, C.P. 38071 22453 Rio de Janeiro, Brazil
and Inst. de Física, Univ. Estadual do Rio de Janeiro, rua São Francisco Xavier 524, Rio de Janeiro, Brazil
[7] Collège de France, Lab. de Physique Corpusculaire, IN2P3-CNRS, 75231 Paris Cedex 05, France
[8] CERN, 1211 Geneva 23, Switzerland
[9] Institut de Recherches Subatomiques, IN2P3 – CNRS/ULP – BP20, 67037 Strasbourg Cedex, France
[10] Now at DESY-Zeuthen, Platanenallee 6, 15735 Zeuthen, Germany
[11] Institute of Nuclear Physics, N.C.S.R. Demokritos, P.O. Box 60228, 15310 Athens, Greece
[12] FZU, Inst. of Phys. of the C.A.S. High Energy Physics Division, Na Slovance 2, 180 40, Praha 8, Czech Republic
[13] Dipartimento di Fisica, Università di Genova and INFN, Via Dodecaneso 33, 16146 Genova, Italy
[14] Institut des Sciences Nucléaires, IN2P3-CNRS, Université de Grenoble 1, 38026 Grenoble Cedex, France
[15] Helsinki Institute of Physics, P.O. Box 64, 00014 University of Helsinki, Finland
[16] Joint Institute for Nuclear Research, Dubna, Head Post Office, P.O. Box 79, 101 000 Moscow, Russian Federation
[17] Institut für Experimentelle Kernphysik, Universität Karlsruhe, Postfach 6980, 76128 Karlsruhe, Germany
[18] Institute of Nuclear Physics,Ul. Kawiory 26a, 30055 Krakow, Poland
[19] Faculty of Physics and Nuclear Techniques, University of Mining and Metallurgy, 30055 Krakow, Poland
[20] Université de Paris-Sud, Lab. de l'Accélérateur Linéaire, IN2P3-CNRS, Bât. 200, 91405 Orsay Cedex, France
[21] School of Physics and Chemistry, University of Lancaster, Lancaster LA1 4YB, UK
[22] LIP, IST, FCUL - Av. Elias Garcia, 14-1^o, 1000 Lisboa Codex, Portugal
[23] Department of Physics, University of Liverpool, P.O. Box 147, Liverpool L69 3BX, UK
[24] Dept. of Physics and Astronomy, Kelvin Building, University of Glasgow, Glasgow G12 8QQ
[25] LPNHE, IN2P3-CNRS, Univ. Paris VI et VII, Tour 33 (RdC), 4 place Jussieu, 75252 Paris Cedex 05, France
[26] Department of Physics, University of Lund, Sölvegatan 14, 223 63 Lund, Sweden
[27] Université Claude Bernard de Lyon, IPNL, IN2P3-CNRS, 69622 Villeurbanne Cedex, France
[28] Dipartimento di Fisica, Università di Milano and INFN-MILANO, Via Celoria 16, 20133 Milan, Italy
[29] Dipartimento di Fisica, Univ. di Milano-Bicocca and INFN-MILANO, Piazza della Scienza 2, 20126 Milan, Italy
[30] IPNP of MFF, Charles Univ., Areal MFF, V Holesovickach 2, 180 00, Praha 8, Czech Republic
[31] NIKHEF, Postbus 41882, 1009 DB Amsterdam, The Netherlands
[32] National Technical University, Physics Department, Zografou Campus, 15773 Athens, Greece
[33] Physics Department, University of Oslo, Blindern, 0316 Oslo, Norway
[34] Dpto. Fisica, Univ. Oviedo, Avda. Calvo Sotelo s/n, 33007 Oviedo, Spain
[35] Department of Physics, University of Oxford, Keble Road, Oxford OX1 3RH, UK
[36] Dipartimento di Fisica, Università di Padova and INFN, Via Marzolo 8, 35131 Padua, Italy
[37] Rutherford Appleton Laboratory, Chilton, Didcot OX11 OQX, UK
[38] Dipartimento di Fisica, Università di Roma II and INFN, Tor Vergata, 00173 Rome, Italy
[39] Dipartimento di Fisica, Università di Roma III and INFN, Via della Vasca Navale 84, 00146 Rome, Italy
[40] DAPNIA/Service de Physique des Particules, CEA-Saclay, 91191 Gif-sur-Yvette Cedex, France
[41] Instituto de Fisica de Cantabria (CSIC-UC), Avda. los Castros s/n, 39006 Santander, Spain
[42] Inst. for High Energy Physics, Serpukov P.O. Box 35, Protvino, (Moscow Region), Russian Federation
[43] J. Stefan Institute, Jamova 39, 1000 Ljubljana, Slovenia and Laboratory for Astroparticle Physics, Nova Gorica Polytechnic, Kostanjeviska 16a, 5000 Nova Gorica, Slovenia,
and Department of Physics, University of Ljubljana, 1000 Ljubljana, Slovenia
[44] Fysikum, Stockholm University, Box 6730, 113 85 Stockholm, Sweden
[45] Dipartimento di Fisica Sperimentale, Università di Torino and INFN, Via P. Giuria 1, 10125 Turin, Italy
[46] INFN,Sezione di Torino, and Dipartimento di Fisica Teorica, Università di Torino, Via P. Giuria 1, 10125 Turin, Italy
[47] Dipartimento di Fisica, Università di Trieste and INFN, Via A. Valerio 2, 34127 Trieste, Italy
and Istituto di Fisica, Università di Udine, 33100 Udine, Italy
[48] Univ. Federal do Rio de Janeiro, C.P. 68528 Cidade Univ., Ilha do Fundão 21945-970 Rio de Janeiro, Brazil
[49] Department of Radiation Sciences, University of Uppsala, P.O. Box 535, 751 21 Uppsala, Sweden
[50] IFIC, Valencia-CSIC, and D.F.A.M.N., U. de Valencia, Avda. Dr. Moliner 50, 46100 Burjassot (Valencia), Spain
[51] Institut für Hochenergiephysik, Österr. Akad. d. Wissensch., Nikolsdorfergasse 18, 1050 Vienna, Austria
[52] Inst. Nuclear Studies and University of Warsaw, Ul. Hoza 69, 00681 Warsaw, Poland
[53] Fachbereich Physik, University of Wuppertal, Postfach 100 127, 42097 Wuppertal, Germany

Received: 10 December 2003 / Revised version: 3 February 2004 /
Published online: 9 March 2004 –

Abstract. The forward-backward asymmetries of the processes $e^+e^- \to Z \to b\bar{b}$ and $e^+e^- \to Z \to c\bar{c}$ were measured from a sample of hadronic Z decays collected by the DELPHI experiment between 1993 and 1995. Enriched samples of $b\bar{b}$ and $c\bar{c}$ events were obtained using lifetime information. The tagging of b and c quarks in these samples was based on the semileptonic decay channels $b/c \to X + \mu$ and $b/c \to X + e$ combined with charge flow information from the hemisphere opposite to the lepton.

Combining the $A_{\rm FB}^{\rm b\bar{b}}$ and $A_{\rm FB}^{\rm c\bar{c}}$ measurements presented in this paper with published results based on 1991 and 1992 DELPHI data samples, the following pole asymmetries were obtained:

$$A_{\rm FB}^{0,\rm b} = 0.1021 \pm 0.0052\ (\rm stat) \pm 0.0024\ (\rm syst)$$
$$A_{\rm FB}^{0,\rm c} = 0.0728 \pm 0.0086\ (\rm stat) \pm 0.0063\ (\rm syst)$$

The effective value of the weak mixing angle derived from these measurements is

$$\sin^2\theta_{\rm W,eff}^{\rm lept} = 0.23170 \pm 0.00097.$$

1 Introduction

The polar angle, θ, of the final state fermion relative to the incoming electron in the reaction $e^+e^- \to f\bar{f}$, at $\sqrt{s} \simeq M_Z$, is distributed according to:

$$\frac{{\rm d}\sigma}{{\rm d}\cos\theta} \propto 1 + \cos^2\theta + \frac{8}{3} A_{\rm FB}^{\rm f\bar{f}} \cos\theta \ . \qquad (1)$$

The coefficient of the $\cos\theta$ term, in the Electroweak Standard Model and for pure Z exchange, is related, at the lowest order, to the vector (v_f) and axial vector (a_f) couplings of the Z to the fermions by:

$$A_{\rm FB}^{\rm f\bar{f}} = \frac{3}{4}\mathcal{A}_e\mathcal{A}_f = \frac{3}{4}\frac{2a_ev_e}{a_e^2+v_e^2}\frac{2a_fv_f}{a_f^2+v_f^2} \ . \qquad (2)$$

Higher order electroweak corrections can be accounted for in the above relations by defining the modified couplings $\bar{v}_f$ and $\bar{a}_f$ and an effective value $\sin^2\theta_{\rm W,eff}^{\rm f}$ of the weak mixing angle:

$$\frac{\bar{v}_f}{\bar{a}_f} = 1 - 4\,|q_f|\sin^2\ \theta_{\rm W,eff}^{\rm f} \qquad (3)$$

where q_f is the electric charge of the fermion in units of the proton charge. The effective value of the weak mixing angle estimated in this paper is the one corresponding to the leptons ($\sin^2\theta_{\rm W,eff}^{\rm lept}$), small contributions specific to the quark sector being corrected for using the program ZFITTER [1].

Because of the values of the Z couplings to fermions, both the forward-backward asymmetry and its sensitivity to $\sin^2\theta_{\rm W,eff}^{\rm lept}$ are larger in the $Z \to q\bar{q}$ channel than in the leptonic ones, thus making the $A_{\rm FB}^{\rm b\bar{b}}$ and $A_{\rm FB}^{\rm c\bar{c}}$ measurements of particular interest. The determination of the quark asymmetries $A_{\rm FB}^{\rm b\bar{b}}$ and $A_{\rm FB}^{\rm c\bar{c}}$ requires:

- the tagging of the Z boson hadronic decays into $b\bar{b}$ and $c\bar{c}$ heavy quark final states;
- the reconstruction of the polar angle of the produced quark/anti-quark axis;
- the orientation of the corresponding axis as a function of the quark direction[1].

The analysis presented here is based on events with identified muons or electrons produced in semileptonic decays of b and c hadrons, referred to as the "lepton sample" in the following. The main parameters used to analyse these events are:

- the kinematic variables associated with the lepton, namely the transverse (p_T) and longitudinal (p_L) momentum with respect to the direction of the closest jet;
- the sign of the lepton electric charge.

Prompt leptons with high p_T and p_L allow the selection of a high purity sample of $e^+e^- \to Z \to b\bar{b}$ events and, at the same time, the discrimination between quark and anti-quark jets on the basis of the charge correlation between the lepton and the parent quark. Decay chains like $b \to c \to l^+$ and $B^0\bar{B}^0$ mixing reduce this charge correlation. Conversely the presence of background and the reduced charge correlations limit the use of the largest fraction of the lepton sample at low p_T and p_L. Two additional variables were used in the present analysis to overcome these limitations in the $A_{\rm FB}^{\rm b\bar{b}}$ measurement:

- a b-tagging variable, based mainly on the probability to observe a given event, assuming the tracks come from the primary vertex, to isolate pure samples of $e^+e^- \to Z \to b\bar{b}$ events;
- a momentum weighted average of the particle charges in the hemisphere opposite to the lepton, to provide an independent estimator of the charge of the primary quark.

By combining the information from the b-tagging and the lepton p_L and p_T, a clean sample of $Z \to c\bar{c}$ could also be selected, allowing the measurement of $A_{\rm FB}^{\rm c\bar{c}}$.

The thrust axis ($\overrightarrow{T}$) of the event, oriented by the jet containing the lepton, was used to determine the direction of the primary quark.

[1] This requirement implies that jets induced by a quark or by an anti-quark have to be distinguished.

The choice of these variables was driven not only by the objective of optimising the statistical precision of the measured asymmetries but also by the capability of calibrating them on the data, thus controlling well the systematics.

The data used here were collected between 1993 and 1995 at energies around the Z peak with the DELPHI detector at LEP. This analysis extends the previously published results based on the events collected in 1990 [2], 1991 and 1992 [3].

After a brief presentation of the DELPHI detector, the event and lepton selections are described. The observables used in the analysis are discussed together with their description by the simulation and the associated sources of systematics. The measurement of the asymmetries $A_{\rm FB}^{\rm b\bar{b}}$ and $A_{\rm FB}^{\rm c\bar{c}}$ is presented in the last sections.

2 Detector description and event selection

2.1 The DELPHI detector

The DELPHI detector has been described in detail in [4]. Only the components which were most relevant to the present analysis are discussed.

The innermost detector in DELPHI was the Vertex Detector (VD), located just outside the LEP beam pipe. It consisted of three concentric cylindrical layers of silicon microstrip detectors at average radii of 6.3, 9.0 and 10.9 cm from the beam line, called the Closer, Inner and Outer layer, respectively. During 1993 it provided only the measurement of the $R\Phi$ [2] coordinate and the polar angle acceptance for a particle crossing all the three layers was limited by the extent of the Outer layer to $44^\circ \leq \theta \leq 136^\circ$ [5]. In 1994 the Closer and the Outer layers were equipped with double sided silicon detectors, also measuring the z coordinate [6]. At the same time the angular acceptance of the Closer layer was enlarged from $30^\circ \leq \theta \leq 150^\circ$ to $25^\circ \leq \theta \leq 155^\circ$. The measured intrinsic precision was about 8 μm for the $R\Phi$ measurement while for z it depended on the polar angle of the incident track, going from about 10 μm for tracks perpendicular to the modules, to 20 μm for tracks with a polar angle of 25°. For charged particle tracks with hits in all three $R\Phi$ VD layers, the impact parameter[3] precision was $\sigma_{R\Phi} = [61/(p\sin^{3/2}\theta) \oplus 20]\mu$m while for tracks with hits in both the Rz layers it was $\sigma_z = [67/(p\sin^{5/2}\theta) \oplus 33]\mu$m, where p is the momentum in GeV/c.

Outside the VD, between radii of 12 cm and 28 cm, the Inner Detector (ID) was located, which included a jet chamber providing up to 24 $R\Phi$ measurements and five layers of proportional chambers with both $R\Phi$ and z information. The ID covered the angular range $29^\circ \leq \theta \leq 151^\circ$. In 1995 a new ID was operational, with the same wire configuration in the inner drift chamber but a wider polar angle acceptance of $15^\circ \leq \theta \leq 165^\circ$.

The VD and the ID were surrounded by the main DELPHI tracking device, the Time Projection Chamber (TPC), a cylinder of 3 m length, of 30 cm inner radius and of 122 cm outer radius. The ionisation charge produced by particles crossing the TPC volume was drifted to the ends of the detector where it was measured in a proportional counter. Up to 16 space points could be measured in the angular region $39^\circ \leq \theta \leq 141^\circ$. The analysis of the pulse height of the signals of up to 192 sense wires of the proportional chambers allowed the determination for charged particles of the specific energy loss, dE/dX, which was used for particle identification.

The Outer Detector (OD) was located between radii of 198 cm and 206 cm and consisted of five layers of drift cells.

In the forward regions two sets of planar wire chambers, at $\pm$ 160 cm and $\pm$ 270 cm in z, completed the charged particle reconstruction at low angle.

The muon identification relied mainly on the muon chambers, a set of drift chambers providing three-dimensional information situated at the periphery of DELPHI after approximately 1 m of iron. One set of chambers was located 20 cm before the end of the hadronic calorimeter (HCAL), two further sets of chambers being outside. At $\theta \simeq 90^\circ$ there were 7.5 absorption lengths between the interaction point and the last muon detector.

In the Barrel part of the detector there were three layers each including two active planes of chambers covering the region $|\cos\theta| < 0.63$. The two external layers overlapped in azimuth to avoid dead spaces. In the Forward part, the inner and the outer layers consisted of two planes of drift chambers with anode wires crossed at right angles. The resolution was 1.0 cm in z and 0.2 cm (0.4 cm) in $R\Phi$ for the Barrel (Forward). In 1994 a further set of chambers (Surround Muon Chambers) was added to cover the region between the Barrel and Forward chambers.

The electromagnetic calorimeter in the barrel region, $|\cos\theta| < 0.73$, was the High density Projection Chamber (HPC), situated inside the superconducting coil. The detector had a thickness of 17.5 radiation lengths and consisted of 144 modules arranged in 6 rings along z, each module was divided into 9 drift layers separated by lead. It provided three-dimensional shower reconstruction. In the forward region, $0.80 < |\cos\theta| < 0.98$, the electromagnetic calorimeter EMF consisted of two disks of 5 m diameter with a total of 9064 lead-glass blocks in the form of truncated pyramids, arranged almost to point towards the interaction region.

2.2 Selection of hadronic events

The selection of charged particle tracks and neutral clusters was performed according to the requirements of Table 1. Hadronic events were then selected with an efficiency of 95% requiring:

[2] In the DELPHI coordinate system, z is along the direction of the incoming electron beam, Φ and R are the azimuthal angle and radius in the xy plane, and θ is the polar angle with respect to the z axis.

[3] The $R\Phi$ impact parameter is defined as the distance between the point of closest approach of a charged particle in the xy plane to the reconstructed primary vertex. The distance in z between this point on the charged particle trajectory and the primary vertex is called the z impact parameter.

Table 1. Requirements on charged particle tracks and neutral clusters for hadronic events selection. On selected events, the energy flow measurement and jets reconstruction were performed with an improved neutral clusters reconstruction, including photons of lower energy in the HPC (down to $\sim 0.3\,\mathrm{GeV}$) and neutral showers of more than 1 GeV reconstructed in the HCAL

charged-particle tracks	polar angle $\lvert\cos\theta\rvert$	< 0.93
	length of track measured inside TPC	$> 30\,\mathrm{cm}$
	impact parameter ($R\Phi$)	$< 5\,\mathrm{cm}$
	impact parameter $\lvert z\rvert$	$< 10\,\mathrm{cm}$
	charged particle momentum	$> 0.2\,\mathrm{GeV}/c$
	relative uncertainty on the momentum	$< 100\%$
neutral clusters	detected by HPC or EMF	
	polar angle $\lvert\cos\theta\rvert$	< 0.98
	HPC (EMF) energy	$> 0.8(0.4)\,\mathrm{GeV}$

– at least 7 accepted charged particles;
– a total measured energy of these charged particles, assuming pion masses, larger that 0.15 times the centre-of-mass energy, $\sqrt{s}$.

A total of 2.7 million hadronic events was selected from 1993–1995 data, at centre-of-mass energies within $\pm\,2\,\mathrm{GeV}$ of the Z resonance mass. A set of 8.4 million simulated hadronic events for years 1993 to 1995 was used, generated using the JETSET 7.3 Parton Shower model [7] in combination with the full simulation of the DELPHI detector. The parameters of the generator were tuned to the DELPHI data as described in [8]. The detailed breakdown of the events used in data and simulation for each year is given in Table 2.

3 Lepton samples

The main kinematical variable used to measure the flavour composition of the leptonic sample was the transverse momentum, p_T, of the lepton with respect to the jet axis. To compute this axis the jet containing the lepton was used, but its direction was reconstructed without the lepton. Jets were built using the JADE algorithm [9] with a scaled invariant mass $y_{cut} = \frac{m_{ij}^2}{E_{vis}^2} \geq 0.01$.

To ensure a good determination of the thrust polar angle, θ_T, the analysis was limited to events with $|\cos(\theta_T)| < 0.9$. For events with more than one lepton candidate, only the highest p_T lepton was used for the $A_{\mathrm{FB}}^{\mathrm{b\bar{b}}}$ and $A_{\mathrm{FB}}^{\mathrm{c\bar{c}}}$ measurement.

The lepton identification has been studied not only by means of special data and simulation samples (for example : $\mu^+\mu^-$, $K^0 \to \pi^+\pi^-$, Compton events) but also using p, p_T and b-tagging[4] cuts to select, in hadronic events, lepton sub-samples with different purity. In practice with only two such lepton sub-samples, two parameters, the efficiency and the purity of the overall sample, can be compared between data and simulation.

Table 2. The number of selected hadronic events for data and simulation

Year	# of events (in 10^3)	
	Data	Simulation
1993	696	2276
1994	1370	4300
1995	662	1829

Table 3. Number of events with at least one lepton candidate for the different years and for the three centre-of-mass energies. The highest p_T lepton is used to classify the event as "muon" or "electron"

Year	Energy	muons	electrons
	89 GeV	6068	4240
1993	91 GeV	28791	21553
	93 GeV	9171	6536
1994	91 GeV	95183	69971
	89 GeV	5147	4062
1995	91 GeV	28600	21786
	93 GeV	8629	6443

The number of lepton candidates for the different years and centre-of-mass energies can be found in Table 3. Details on the lepton identification and on the sample composition are given in the next two sub-sections.

3.1 Muon sample

For the muon identification the tracks reconstructed in the central detectors were used to define a path along which

[4] The b-tagging method and its calibration will be presented in detail in Sect. 4. b-tagged and anti-b-tagged samples refer, respectively, to the purer and to the most contaminated b sub-samples as defined in Sect. 4. The b-tagging is used in this section to estimate the purity of the electron sample but is only used as a cross-check for the muon sample. For this reason to avoid any sizable correlation in the tuning of the simulation, the b-tagging calibration used in this section was based on events from the muon sample alone.

hits in the muon chambers were looked for. The identification algorithm has been described extensively in [3]. Muon candidates with a momentum, p, above 2.5 GeV/c and in the region of good geometrical acceptance were selected. The muon polar angle θ_μ was required to be in the region $0.03 < |\cos\theta_\mu| < 0.6$ or $0.68 < |\cos\theta_\mu| < 0.93$. Only for a small fraction of the 1994 data sample the Surround Muon Chambers, which filled the gap between the barrel and forward detectors, were able to provide useful muon identification.

The muon identification efficiency was measured in $Z \to \mu^+\mu^-$, $Z \to \tau^+\tau^-$and $\gamma\gamma \to \mu^+\mu^-$ events, yielding on average about 0.85 for 45 GeV/c muons and 0.83 for momenta between 10 and 5 GeV/c.

In order to extract $A_{\rm FB}^{\rm b\bar{b}}$ and $A_{\rm FB}^{\rm c\bar{c}}$ from the observed asymmetry the absolute lepton efficiency is not required, only a correct description of the sample purity is needed. The contamination from misidentified hadrons arises partly from the decay of pions and kaons and, for momenta above 3 GeV/c, mostly from energetic hadrons interacting at the end of the calorimeter and generating punch-throughs. K_S^0 particles decaying into two pions were used to measure the rate of pion misidentification above 3 GeV/c showing that the fraction of pions misidentified as muons was $1.79 \pm 0.09 \pm 0.05$ and $1.41 \pm 0.10 \pm 0.03$ times bigger in data than in the simulation for the barrel and the forward regions respectively. Muons from pion decays were subtracted from the misidentified sample to compute the numbers quoted above. The first error is due to the limited statistics, the second corresponds to a 15% change in the contamination of muons from pion decays. The fraction of muons from π and K decays present in the selected muon sample was determined to this precision by comparing the size of two muon sub-samples in hadronic events selected by p,p_T cuts[5].

To measure further the sample composition directly from the data, the number of muon candidates, normalised to the number of hadronic Z decays, was compared between data and simulation in sub-samples enriched in prompt muons or background by different sets of selections in p, p_T or b-tagging. The stability of the misidentification correction quoted above was measured as a function of p, p_T and θ in b and anti-b-tagged samples. No discrepancy was observed outside expected statistical fluctuations. For example in the anti-b-tagged sub-sample, which had a purity of 30% in leptons from heavy flavour decay, a data/simulation comparison for 28 bins in momentum had a 27% χ^2 probability. In this same sub-sample the 6.6% excess of positive particles due to the difference between the K^+ and K^- cross-sections in the detector, was also perfectly described with a statistical precision of $\pm$ 0.5%. These studies confirmed the correct description in the tuned simulation of the different sources of background within the uncertainties quoted above.

[5] The first one was selected with $p > 2.5$ GeV/c and $p_T < 0.7$ GeV/c and the second one with $p > 4$ GeV/c and $p_T > 0.7$ GeV/c, the two samples having respectively 19% and 4% of muons from π and K decays.

Table 4. Full 1993–1995 lepton sample composition. The leptons from heavy flavour decays, when the heavy flavour quark was coming from a gluon splitting, are counted in "other", line "h)". The total efficiency to select a muon or an electron from the process "a)"is respectively (44.7 ± 0.2)% and (35.4 ± 0.4)% including all effects (momentum cuts and detector inefficiencies) except the efficiency to select hadronic events

Lepton candidate source	Sample composition in %	
	μ	e
Lepton from b hadron decay : "same sign"	**32.5**	**35.1**
a) $b \to l^-$	29.0	31.6
b) $b \to \tau \to l^-$	1.0	1.0
c) $b \to \bar{c} \to l^-$; $b \to \bar{c} \to \tau \to l^-$	2.5	2.5
Lepton from b hadron decay : "opposite sign"	**11.8**	**11.7**
d) $b \to c \to l^+$; $b \to c \to \tau \to l^+$		
Lepton from b hadron decay : other source	**0.3**	**0.3**
e) $b \to J/\Psi \to l^+l^-$		
Lepton from c decay	**16.8**	**15.9**
f) $c \to l^+$; $c \to \tau \to l^+$		
Background	**38.6**	**37.0**
g) Misidentification	26.3	18.2
h) Light mesons decay / converted gammas / other	12.3	18.8

The comparison between data and simulation for the $\cos\theta_\mu$ distribution is presented in Fig. 1. The muon sample composition is given in Table 4.

3.2 Electron sample

The electron candidates of momentum higher than 2 GeV/c were identified in the barrel ($0.03 < |\cos\theta_e| < 0.7$) by combining the electromagnetic shower information from the HPC and the track ionisation measured by the TPC, with a neural network. In the forward region ($0.7 < |\cos\theta_e| < 0.9$) only the ionisation measured by the TPC was used. Mainly due to the large amount of material in front of the EMF, the calorimetric information in the forward regions was not used to identify electrons.

Electrons in the barrel region

In the barrel the contamination and efficiency of the electron sample was tuned in the simulation using two subsamples with $p > 3$ GeV/c and a b or anti-b-tag. Their content of misidentified electrons was respectively 27% and 89%. The efficiency was found to be correctly described by the simulation, in agreement with a study based on Compton scattering and photon conversion samples [10]. The misidentification probability was found in the data to be a factor 0.9 lower than that in the simulation, with variations within a few percent as a function of the year and angular region. A study based on sub-samples selected by p and p_T cuts gave compatible results. The relative precision on this correction was estimated to be $\pm$5%.

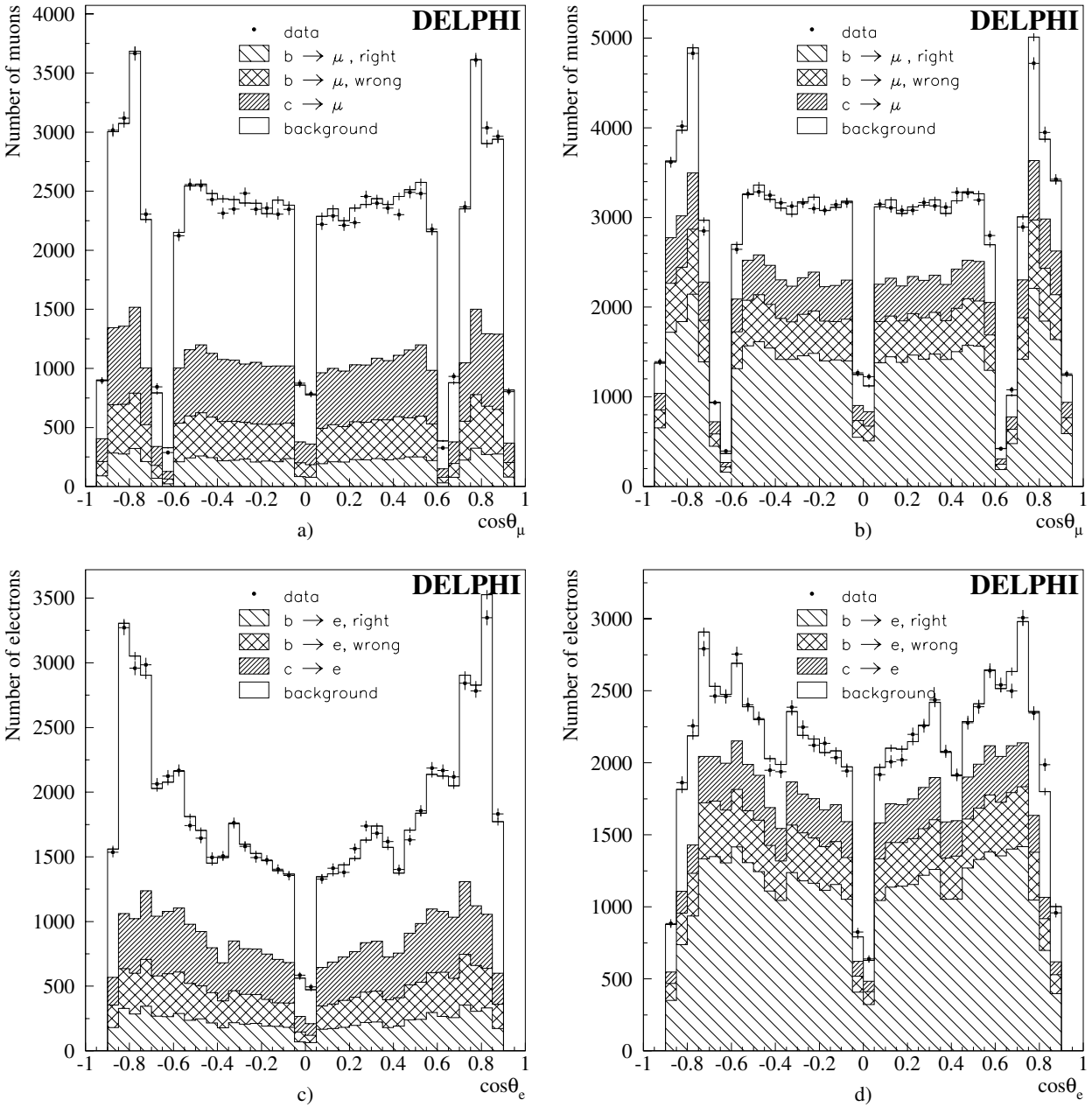

Fig. 1a–d. $\cos\theta$ distribution for muon, upper plots, and electron, lower plots, candidates. The lepton candidates have $p_T < 0.7\,\mathrm{GeV}/c$ in **a** , **c** and $p_T > 0.7\,\mathrm{GeV}/c$ in **b** , **d** corresponding to samples enriched in background and signal respectively. The "$b \to \mu/e$ right (wrong)" samples correspond to leptons with the same (opposite) sign as the primary b parton (see Sect. 6.1). Converted photons cause the strong $\cos\theta_e$ dependence of the background in the **c** plot. Only the statistical errors are quoted in these plots. The systematics on the samples composition considered in the text are enough to cover the few discrepancies observed between the data and the simulation

The number of selected electron candidates in a low p ($p < 3\,\mathrm{GeV}/c$) and p_T ($p_T < 1\,\mathrm{GeV}/c$) region for anti-b-tagged events agreed between data and simulation for the standard and low converted gamma rejections (with converted gamma rejections of 90% and 75% respectively). This study was statistically compatible with a correct description of the converted gamma content of the electron sample at a ± 10% level.

Electrons in the forward regions

In the forward regions, where only the ionisation measured by the TPC was used, the misidentification could be studied with the muon sample, muons and pions having almost the same ionisation signature in the TPC. This showed the need to increase the misidentification by a factor 1.12±0.07 in the simulation. The amount of electron from converted photons was determined with the help of the b-tagging and

p, p_T requirements as above. This amount was found to be correctly described by the simulation for the different years within a precision better than ± 10%.

The comparison between the data and the simulation for the $\cos\theta_e$ distribution is presented in Fig. 1. The composition of the electron sample is quoted in Table 4.

4 Use of the b-tagging information

To improve the separation between heavy and light flavours a b-tagging technique developed for the measurement of R_b, the partial width of Z into $b\bar{b}$ pairs, was used [11].
Each event was divided into two hemispheres according to the direction of the thrust axis, and the b-tagging probability for a hemisphere to contain a b quark was given by the jet with the highest b-tagging probability in the hemisphere.

The tagging technique was based on the combination of up to four discriminating variables, x_i (i=1 to 4), defined for each jet:

- the jet lifetime probability, constructed from the positively signed impact parameters of all tracks included in a jet, is built from the probabilities to observe a given set of impact parameters, assuming the tracks come from the primary vertex;
- the effective mass of the system of particles assigned to the secondary vertex [6];
- the rapidity of tracks associated to the secondary vertex with respect to the jet direction;
- the fraction of the jet energy carried by charged particles from the secondary vertex.

The correct description of these variables by the simulation is shown in [11].

For each jet containing a secondary vertex, the four variables x_i were then combined into a single tagging variable y by means of their probability density functions $f_i^{uds}(x_i)$, $f_i^c(x_i)$, $f_i^b(x_i)$, for uds, c and b quarks respectively, as determined from simulation studies:

$$y = n_c \prod \frac{f_i^c(x_i)}{f_i^b(x_i)} + n_{uds} \prod \frac{f_i^{uds}(x_i)}{f_i^b(x_i)},$$

n_c, n_{uds} being the fractions of c-jets and uds-jets with a reconstructed secondary vertex normalised by the relation: $n_c + n_{uds} = 1$. Only the first variable was used if no secondary vertex was reconstructed. Hemispheres with a jet containing a b-quark were characterised by a large value of the variable $\eta_{\rm HEM} = -\log_{10} y$.

The value of the tagging variable for the whole event was computed from the corresponding values obtained in each hemisphere as:

$$\eta_{\rm EVT} = \max(\eta_{\rm HEM1}, \eta_{\rm HEM2}).$$

The sample composition determination, as a function of the value of $\eta_{\rm EVT}$, was needed to extract $A_{\rm FB}^{\rm b\bar{b}}$ and $A_{\rm FB}^{\rm c\bar{c}}$ from the raw asymmetries. Since a separate tag for each hemisphere was used, the sample composition could be derived from the data themselves with minimum input from the simulation by using a technique similar to the single tag versus double tag method of the R_b analysis [11].

For events with the thrust axis situated within the barrel acceptance ($|\cos\theta_T| < 0.7$), the distribution of the hemisphere b-tagging variable $\eta_{\rm HEM}$ was divided into three intervals corresponding, respectively, to events enriched in uds (I), c (II) or b (III) flavours. For this low number of intervals a direct measurement of their content in term of uds, c and b can be implemented in the data as follows.

In each interval j the fraction $f_E^{(j)}$ of events with at least one hemisphere in that interval and the fraction $f_H^{(j)}$ of hemispheres in the interval itself, were expressed by the following relations:

$$\begin{aligned} f_E^{(j)} &= \sum_q r_q \left(2\varepsilon_q^{(j)} - \varepsilon_{D,q}^{(j)}\right) \\ &= \sum_q r_q \varepsilon_q^{(j)} \left[2 - \rho_q^{(j)} - \varepsilon_q^{(j)}(1-\rho_q^{(j)})\right], \\ f_H^{(j)} &= \sum_q r_q \varepsilon_q^{(j)}, \end{aligned} \tag{4}$$

where $\varepsilon_q^{(j)}$ were the fractions of hemispheres in the $j-$th interval for the flavour q ($q = uds, c, b$), and the correlations $\rho_q^{(j)} = (\varepsilon_{D,q}^{(j)} - \varepsilon_q^{(j)\,2})/(\varepsilon_q^{(j)}(1-\varepsilon_q^{(j)}))$ accounted for the probability ($\varepsilon_{D,q}^{(j)}$) of having both hemispheres in that interval. The variables r_q stand for the fractions of $Z \to q\bar{q}$ events in the selected leptonic sample.
The requirement of an identified lepton in the final state strongly enhanced the fraction of events with a Z decaying into heavy quark pairs. Therefore the fractions r_q were obtained from R_q, the Standard Model partial decay widths of the Z, via the relation

$$r_q = R_q \frac{e_{q,\ell}}{e_{{\rm had},\ell}} \quad q = uds, c, b \tag{5}$$

where $e_{q,\ell}$ was the flavour dependent hadronic selection efficiency, taken from the simulation, and $e_{{\rm had},\ell} = \sum_{uds,c,b} \times R_q e_{q,\ell}$. To determine the fractions $\varepsilon_{q,RD}^{(j)}$ in real data for the different intervals, it has been assumed that they differ only slightly from the ones in the simulation, $\varepsilon_q^{(j)}$:

$$\varepsilon_{q,RD}^{(j)} = \varepsilon_q^{(j)}(1 + \delta_q^{(j)})$$

In the approximation, confirmed by the data, of small corrections $\delta_q^{(j)}$, the set of Equations (4), including the

[6] A secondary vertex was required to contain at least 2 tracks not compatible with the primary vertex and to have $L/\sigma_L > 4$ where L is the distance from the primary to the secondary vertex and σ_L is its error. Each track assigned to the secondary vertex should have at least one measurement in the VD and at least 2 tracks should have measurements in both $R-\Phi$ and $R-z$ planes of the VD.

closure relations on the fractions $\varepsilon^{(j)}_{q,RD}$ and $\varepsilon^{(j)}_q$, gives at first order in $\delta^{(j)}_q$:

$$\sum_q r_q \varepsilon^{(j)}_q \left[2 - \rho^{(j)}_q - 2\varepsilon^{(j)}_q(1-\rho^{(j)}_q)\right]\delta^{(j)}_q$$
$$= f^{(j)}_E - \sum_q r_q \varepsilon^{(j)}_q \left[2 - \rho^{(j)}_q - \varepsilon^{(j)}_q(1-\rho^{(j)}_q)\right], \quad (6)$$

$$\sum_q r_q \varepsilon^{(j)}_q \delta^{(j)}_q = f^{(j)}_H - \sum_q r_q \varepsilon^{(j)}_q, \quad (7)$$

$$\sum_j^{N_{\rm int}} \varepsilon^{(j)}_q \delta^{(j)}_q = 0, \quad (8)$$

where $\rho^{(j)}_q$ and $\varepsilon^{(j)}_q$ were taken from the simulation. For $N_{\rm int} = 3$ b-tagging intervals there are in total 9 unknowns $\delta^{(j)}_q$ and 9 equations. The rank of the matrix of the coefficients is 8 so that one input $\delta^{(j)}_q$ was required[7]. For $N_{\rm int} = 2$ and merging together 2 flavours, the system reduces to 6 equations and 4 unknowns. Since the rank of the matrix of the coefficients is 4 the system has one exact solution[8]. Therefore the $\delta^{(j)}_q$ for $N_{\rm int} = 3$ were obtained in two steps. First we combined together the two highest bins of $\eta_{\rm HEM}$, merged the c and b contributions and solved this reduced system with 4 unknowns. Then the full system was solved fixing $\delta^{(\rm I)}_{uds}$ to the value obtained in the previous step.

For events with $0.7 < |\cos\theta_T| < 0.85$, because of the reduced performances of b-tagging in the forward region, only the reduced system with 4 unknowns was solved. No b-tagging information was used for events with $|\cos\theta_T| > 0.85$ [9].

Errors on $\delta^{(j)}_q$ due to the finite statistics of the simulated sample were estimated in the following way. For each flavour q, we considered the two dimensional distributions $\{\eta_{\rm HEM1}, \eta_{\rm HEM2}\}$ which could be derived from the original one in the simulation by adding -1, 0, and $+1$ standard deviations to the content of each interval. This was done conserving the total number of events of that flavour and with the standard deviations given by the multinomial distribution. For each configuration the coefficients $\varepsilon^{(j)}_q$, $\rho^{(j)}_q$ in (4) were recomputed and then the system solved. The spread of the different solutions for the $\delta^{(j)}_q$ was considered as the simulation statistical error on these corrections.

As a cross check of the method, the simulated sample was divided into 6 different sub-samples of equal size. For each sub-sample, the system was solved and the uncertainty on the solutions was evaluated by using the procedure described above. The spread of the solutions in the subsets was found to be in agreement with the estimation of the error. The corrections $1 + \delta^{(j)}_q$ to the simulation fractions found for the 1994 sample together with the error due to the finite simulation statistics are shown in Table 5. For all the samples, the corrections $\delta^{(\rm III)}_{uds}$ were found to be compatible with zero indicating a good control of the background level in the region most relevant in this measurement. The fractions $\varepsilon^{(III)}_b$ were found instead 2–4 % higher in the data than in the simulation.

Table 5. Values of the fractions ($\varepsilon^{(j)}_q$), obtained from the simulation, and of their respective corrections ($1 + \delta^{(j)}_q$), fitted on real data, using 1994 event samples

bin	I	II	III
(dominant flavour)	(uds)	(c)	(b)
Barrel region			
$\varepsilon^{(j)}_{uds}$	0.71	0.23	0.06
$1 + \delta^{(j)}_{uds}$	1.019 ± 0.003	0.950 ± 0.017	0.986 ± 0.072
$\varepsilon^{(j)}_c$	0.45	0.34	0.21
$1 + \delta^{(j)}_c$	0.986 ± 0.007	1.046 ± 0.013	0.956 ± 0.031
$\varepsilon^{(j)}_b$	0.13	0.18	0.69
$1 + \delta^{(j)}_b$	0.970 ± 0.009	0.946 ± 0.006	1.020 ± 0.002
Forward regions			
$\varepsilon^{(j)}_{uds}$	0.70	.30	
$1 + \delta^{(j)}_{uds}$	1.000 ± 0.009	1.000 ± 0.021	
$\varepsilon^{(j)}_{bc}$	0.36	.64	
$1 + \delta^{(j)}_{bc}$	$.931 \pm 0.008$	1.039 ± 0.005	

For the system with $N_{\rm int} = 3$ the predicted correlations have a sizable value only for $\rho^{(\rm III)}_b$ ($= 0.027 \pm 0.005$ in 1994). The detector and QCD origins of such correlations have been studied in detail in [11]. In the present analysis even a 100% change in the predicted correlation has a small impact on the estimated data sample composition. The variation induced is of the same order as the one associated to the statistical uncertainty on $\delta^{(j)}_q$.

For the system with $N_{\rm int} = 2$ the predicted correlations were up to ~ 0.1 for the b/c flavours and still compatible with zero for the uds sample. The high value of $\rho^{(j)}_{bc}$ obtained in this case is a pure artifact of the merging of the b and c samples and is just related, at first order, to the difference in tagging efficiency of b and c.

The merging of b and c for $N_{\rm int} = 2$ is justified by the fact that for the b-tagging intervals used in this case, the $\delta^{(j)}_q$ corrections are mainly related to the difference in the description of the detector response between real data and simulation and not to the details of the b and c physics. This is supported by the fact that in the interval I dominated by uds, which is the same both for $N_{\rm int} = 2$ and $N_{\rm int} = 3$, the corrections $\delta^{(I)}_c$ and $\delta^{(I)}_b$ in the barrel are compatible (cf. Table 5). To evaluate possible biases from this merging procedure, another system, also with $N_{\rm int} = 2$, was built starting from the original one with $N_{\rm int} = 3$ but now combining the two lowest bins of $\eta_{\rm HEM}$, bins I and II, and merging the uds and c flavours. The

[7] As by construction $\sum_j^{N_{\rm int}} \varepsilon^{(j)}_q = 1$ implies $\sum_j^{N_{\rm int}} f^{(j)}_H = 1$, one equation among the Equations (7) and (8) can be deduced from the other.

[8] For $N_{\rm int} = 2$, we have by definition $\rho^{(1)}_q = \rho^{(2)}_q$ which makes in this case the two equations associated to (6) equivalent.

[9] For the 1993 data sample, due to the reduced length of the micro-vertex detector, the b-tagging was performed only down to $|\cos\theta_T| < 0.81$.

Table 6. Values of $\sigma_{Q_{\mathrm{jet},l}}$, f and $\overline{Q}_{\mathrm{jet},l}$ in the barrel for the subsample enriched in b, fitted in the data and in the simulation before tuning in 1994. It should be noticed that, because of the constraint expressed by (9), f and $\overline{Q}_{\mathrm{jet},l}$ are fully anti-correlated. The first quoted error corresponds to the analysed statistics and the other, in the case of data, to systematics

	$\sigma_{Q_{\mathrm{jet},l}}$	f in %		$\overline{Q}_{\mathrm{jet},l}$	
		μ sample	e sample	μ sample	e sample
Data	$.2842 \pm .0004 \pm .0021$	$68.4 \pm .6 \pm .6$	$70.2 \pm .8 \pm .6$	$.099 \mp .003 \mp .003$	$.098 \mp .004 \mp .003$
Sim.	$.2894 \pm .0003$	$69.3 \pm .4$	$71.1 \pm .4$	$.103 \mp .002$	$.101 \mp .002$

changes found in $A_{\mathrm{FB}}^{\mathrm{b\bar{b}}}$ and $A_{\mathrm{FB}}^{\mathrm{c\bar{c}}}$ were taken conservatively as systematic errors (cf. Sect. 7).

5 Use of the jet charge information.

The jet charge measured in the event hemisphere, opposite to the lepton, provides an additional information on the charge of the parton from which the lepton originates. This information is particularly relevant for events with a low p_T lepton to be still able to distinguish between $b \to l^-$ and $b \to c \to l^+$ and for events with a high p_T lepton to tag $B^0\bar{B}^0$ oscillations. The jet charge was built by means of a momentum-weighted (p_i) average of the charges (q_i) of the charged particles in the hemisphere opposite to the lepton:

$$Q_{\mathrm{opp}} = \frac{\sum_{\mathrm{hem}} q_i |\overrightarrow{p_i} \cdot \overrightarrow{T}|^K}{\sum_{\mathrm{hem}} |\overrightarrow{p_i} \cdot \overrightarrow{T}|^K}$$

with the event divided into two hemispheres by a plane perpendicular to the thrust axis $\overrightarrow{T}$.

With this definition the information coming from the tracks in the lepton hemisphere was not used in order to avoid the strong bias in the topology due to the presence of a lepton. Based on the work presented in [12] $K = 0.8$ was chosen to optimise the $b/\bar{b}$ separation. We restricted the use of the jet charge to the events with the thrust axis in the barrel ($|\cos\theta_T| < 0.7$) and belonging to the lepton subsample enriched in b (bin III according to the definition given in Sect. 4).

The distribution of the total event jet charge in the hadronic decays of the Z turned out to be systematically displaced from zero ($\sim +0.01$), due to the hadronic interactions of particles inside the detector. It was checked that this shift was independent of the event flavour in each b-tag bin and is corrected for, separately in the data and in the simulation, as a function of the thrust axis of the event. After this correction it was possible to treat in a consistent way positive and negative leptons, by using, as $b/\bar{b}$ discriminating variable, the product of the lepton charge times the opposite jet charge, $Q_\ell \times Q_{\mathrm{opp}}$. For a pure sample of leptons coming from $Z \to b\bar{b}$ decays, $Q_\ell \times Q_{\mathrm{opp}}$ has a Gaussian distribution centred at negative (positive) values in case of right (wrong) sign correlation between the lepton and the b parton from the opposite hemisphere. In the following this central value will be quoted as $\pm\overline{Q}_{\mathrm{jet},l}$ and the width of the Gaussian as $\sigma_{Q_{\mathrm{jet},l}}$. After normalisation by the total number of leptons, the integral of the Gaussian with the negative mean will be quoted as f, the integral of the other Gaussian being then equal to $1 - f$.

A procedure of self calibration of $Q_\ell \times Q_{\mathrm{opp}}$ with the data was used so as not to rely on the simulation for the jet charge description. It also allowed the fraction f to be more independent of the precise knowledge of the $B^0\bar{B}^0$ mixing or of the branching fractions for the direct ($b \to \ell^-$) and cascade ($b \to c \to \ell^+$) semileptonic decays.

The first step of the jet charge self calibration consisted in the tuning of the simulation in order to reproduce the total event jet charge distribution measured in data. The total event jet charge measured in the full sample of b-tagged hadronic decays could be used. This distribution gives a direct estimate of $\sigma_{Q_{\mathrm{jet},l}}$ [12].

As a second step the values of f and $\overline{Q}_{\mathrm{jet},l}$ were obtained by a double Gaussian fit of $Q_\ell \times Q_{\mathrm{opp}}$ in the data. This has been done for each year for muon and electron separately, after subtracting the background predicted by the simulation. The statistical sensitivity of the fit was improved by reducing the number of fitted parameters using the following constraint:

$$\langle Q_\ell \times Q_{\mathrm{opp}} \rangle = (1\text{–}2f)\overline{Q}_{\mathrm{jet},l}. \qquad (9)$$

This constraint is derived from the definition of the two Gaussian distributions introduced above.

Subsequently the jet charge values in the simulation were corrected to reproduce the measured distribution of mean, $\overline{Q}_{\mathrm{jet},l}$, and width, $\sigma_{Q_{\mathrm{jet},l}}$. Moreover, in each lepton subsample, the events were re-weighted in order to reproduce the fitted value of the fraction of right sign leptons, f. After this calibration the simulation describes the data correctly as can be seen in Fig. 2; event sub-samples enriched, by kinematical cuts, in leptons from different origin like $b \to l^-$ in the high p_T region or $b \to c \to l^+$ in the low p_T one, are well described even if they have quite different values for $\langle Q_\ell \times Q_{\mathrm{opp}} \rangle$. Figure 2 gives a good consistency check of the overall simulation tuning regarding the lepton sample composition.

There are two sources of uncertainty related to the jet charge self calibration method (see Table 6) :

- the $\sigma_{Q_{\mathrm{jet},l}}$, f and $\overline{Q}_{\mathrm{jet},l}$ are measured with a statistical uncertainty in the simulation and in the data,
- the $\sigma_{Q_{\mathrm{jet},l}}$, f and $\overline{Q}_{\mathrm{jet},l}$ values are extracted from the data after subtraction of the uds and c contamination. This subtraction, as it relies on estimates from the simulation, induces systematic errors.

These errors have been estimated using samples enriched in uds or c events, corresponding to the b-tagged

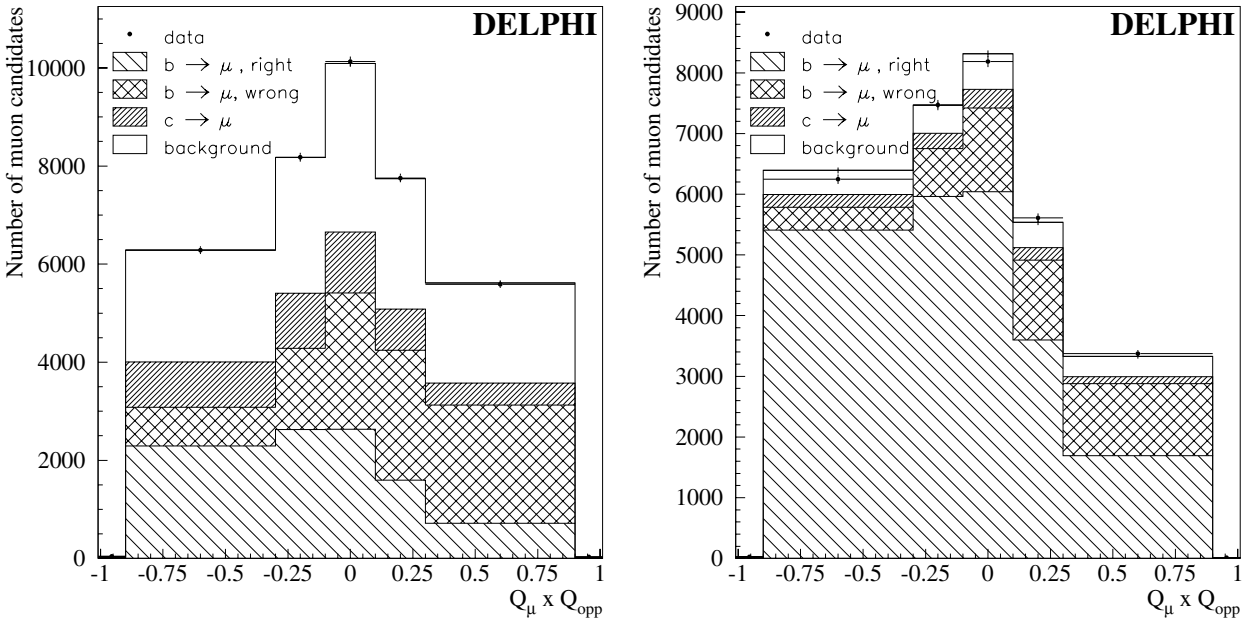

Fig. 2. Jet charge distribution for the full muon sample. The muon candidates have $p_T < 1.3\,\mathrm{GeV}/c$ and $p < 7\,\mathrm{GeV}/c$ (left) and $p_T > 1.3\,\mathrm{GeV}/c$ (right) corresponding to samples enriched in $b \to c \to \mu^+$ or $b \to \mu^-$ events respectively

events in bins (I) or (II). In such samples any difference in the event charge or jet charge distributions between data and the tuned simulation was entirely attributed to an imperfect description in the simulation of the *uds* or *c* events. Using a new description of the event or jet charge for *uds* or *c* events to fix these differences, new values of $\sigma_{Q_{\mathrm{jet},l}}$ or f and $\overline{Q}_{\mathrm{jet},l}$ were then estimated. The biggest changes in $\sigma_{Q_{\mathrm{jet},l}}$, f and $\overline{Q}_{\mathrm{jet},l}$ observed have been considered as systematic errors.

6 The fit of the asymmetries

The $A_{\mathrm{FB}}^{\mathrm{b\bar{b}}}$ and $A_{\mathrm{FB}}^{\mathrm{c\bar{c}}}$ asymmetries were extracted from a minimum χ^2 fit to the observed charge asymmetry, $A_{FB}^{\mathrm{obs},i}$, defined as:

$$A_{FB}^{\mathrm{obs},i} = \frac{N^-(i) - N^+(i)}{N^-(i) + N^+(i)}$$

where $N^+(i)$ and $N^-(i)$ are the numbers of events with an identified lepton in the i-th bin with, respectively, a positive and a negative electrical charge.

Four variables were used for binning the sample: $\cos\theta_T$, which accounted for the polar angle dependence of the asymmetries, and three multivariate classification parameters, chosen to have bins enriched with leptons from a single origin. These last three parameters allowed the statistical errors of the $A_{\mathrm{FB}}^{\mathrm{b\bar{b}}}$ and $A_{\mathrm{FB}}^{\mathrm{c\bar{c}}}$ measurements to be reduced.

6.1 The multivariate parameters

The observables entering the multivariate parameters, whose values depend on the origin of the lepton candidates, were chosen to be:

- the transverse (p_T) and longitudinal (p_L) momenta of the lepton;
- the event b-tagging, η_{EVT};
- the product of the lepton charge times the jet charge of the opposite hemisphere, $Q_\ell \times Q_{\mathrm{opp}}$.

Starting from these observables a multivariate tagging of the lepton origin was built by considering four classes:

1. b_r : leptons from b hadron decays in $Z \to b\bar{b}$ events with the right sign correlation (same sign) with respect to the primary b quark;
2. b_w : leptons from b hadron decays in $Z \to b\bar{b}$ events with the wrong sign correlation (opposite sign) with respect to the primary b quark;
3. c : prompt leptons from c decays in $Z \to c\bar{c}$;
4. bkg : other processes (misidentified hadrons, leptons from light hadron decay, electron and positron from photon conversion and leptons from heavy flavour hadron decays where the heavy flavour quarks were produced by gluon splitting).

The sign correlation mentioned here refers to the one between the lepton charge and the $b/\bar{b}$ flavour at production and therefore it includes possible effects due to $B^0\bar{B}^0$ mixing (cf. Sect. 6.3 for a more extended discussion on the mixing). The probability densities $p_k^{p_T,p_L}$ and $p_k^{\mathrm{btag,jet-ch}}$ of observing a set of (p_T, p_L) and $(\eta_{\mathrm{EVT}}, Q_\ell \times Q_{\mathrm{opp}})$ values for a lepton from the class k were computed by using two-dimensional distributions from the tuned simulation. A likelihood ratio $\mathcal{P}_k$ was built to estimate the probability corresponding to a given set of values within a class:

$$\mathcal{P}_k = \frac{N_k p_k^{p_T,p_L} p_k^{\mathrm{btag,jet-ch}}}{\Sigma_{k'} N_{k'} p_{k'}^{p_T,p_L} p_{k'}^{\mathrm{btag,jet-ch}}}$$

where N_k ($N_{k'}$) is the total number of leptons from the class k (k'). The scaling of the likelihood ratio by N_k takes

into account the relative weights of each class. Neglecting some of the correlations between the observables, such a definition identifies $\mathcal{P}_k$ as the fraction of lepton candidates with a given set of $p_T, p_L, \eta_{\rm EVT}$ and $Q_\ell \times Q_{\rm opp}$ belonging to the class k.

This technique, used for the multivariate classification, extends that in [11] by considering probabilities in two dimensions and takes into account part of the correlations between pairs of observables.

In order to consider the possible improvement by taking into account all possible correlations, an approach based on a classification with a neural network was also tried. The results obtained were in good agreement with those from the multivariate approach but had a slightly worse statistical precision. The multivariate approach was chosen as it allowed, for the small number of observables used, a simpler control of the analysis and an optimal use of the available simulation statistics.

The $\mathcal{P}_{b_r}, \mathcal{P}_{b_w}$ and $\mathcal{P}_c$ distributions for muons and electrons are shown in Fig. 3.

6.2 Measurement of $A_{\rm FB}^{\rm b\bar{b}}$ and $A_{\rm FB}^{\rm c\bar{c}}$

The asymmetries $A_{\rm FB}^{\rm b\bar{b}}$ and $A_{\rm FB}^{\rm c\bar{c}}$ were extracted from a χ^2 fit to the observed asymmetries $A_{FB}^{{\rm obs},i}$ over the different bins of the ($\cos\theta_T$, $\mathcal{P}_{b_r}$-$\mathcal{P}_{b_w}$, $\mathcal{P}_c$) parameter space:

$$\chi^2 = \sum_i \frac{\left(\left(\left(f^i_{b_r} - f^i_{b_w}\right) A_{\rm FB}^{\rm b\bar{b}} + f^i_c A_{\rm FB}^{\rm c\bar{c}} + f^i_{bkg} A_{FB}^{bkg,i}\right) W^i_{\theta_T} - A_{FB}^{{\rm obs},i}\right)^2}{\sigma_i^2} \quad (10)$$

where:

- $W^i_{\theta_T} = \frac{8}{3}\frac{1}{N^i_{\rm data}} \sum_{j=1}^{N^i_{\rm data}} \frac{\cos\theta^j_T}{1+(\cos\theta^j_T)^2}$ takes into account the dependence of the asymmetry on the polar angle;
- σ_i is the statistical error including contributions from both data ($A_{FB}^{{\rm obs},i}$) and simulation (f^i_k,$A_{FB}^{bkg,i}$);
- f^i_k are the different fractions in each bin determined from the tuned simulation.

To optimise the use of the available statistics, the multivariate variables were computed separately for the different years and lepton samples and all samples were merged for the χ^2 fit. The data binning in the parameter space was done to have the same number of events per bin, ~ 100, ~ 180 and ~ 150 events for $\sqrt{s} = 89.43\,\text{GeV}$, $91.22\,\text{GeV}$ and $92.99\,\text{GeV}$ respectively.

Due to the opposite sign in the contribution of the b_r and b_w classes to the b asymmetry only the difference between the fractions of b_r and b_w classes matter in practice. It's why the equi-populated bins for the χ^2 fit were defined by using the combined variable $\mathcal{P}_{b_r} - \mathcal{P}_{b_w}$ and $\mathcal{P}_c$. A possible third sampling corresponding to $\mathcal{P}_{bkg}$ has been found of marginal interest, mainly due to the closure relation on the $\mathcal{P}_k$, and has not been used for the present fit.

A sign correlation between the lepton candidate and the parent quark can exist also for the misidentified leptons thus leading to non-zero values for the background asymmetry $A_{FB}^{bkg,i}$. Furthermore, since this correlation increases with the particle momentum and as a function of b-tagging value, $A_{FB}^{bkg,i}$ must be known in each bin. To optimise the statistical precision of the estimated $A_{FB}^{bkg,i}$, the same factorisation technique as in the previous analysis [3] was adopted: the simulation was only used to determine the charge correlation between the background and the initial quark in each bin, while the quark asymmetries were set to their Standard Model expectation for background in light quark events[10] or to the fitted parameters $A_{\rm FB}^{\rm b\bar{b}}$, $A_{\rm FB}^{\rm c\bar{c}}$ for background in b or c events.

6.3 Effect of the $B^0\bar{B}^0$ mixing

The $B^0\bar{B}^0$ mixing reduces the charge correlation between the initial $b/\bar{b}$ produced from the Z decay and the lepton issued from the B hadron semileptonic decay. The size of the change depends on the proper decay time of the B hadron and on its type, resulting in different values of the effective mixing in the different bins of the lepton sample, for the following reasons:

- the B^0_d and B^0_s fractions in the b sample are not the same for direct or cascade decay leptons due to differences between the $D^+/D^0/D_s$ production rates from the different B hadrons; this introduces, for example, a variation of the effective mixing as a function of p_T;
- the use of the b-tagging biases the content of the bins in terms of proper decay time, thus introducing sizable changes in the effective mixing;
- the sign correlation between the lepton and the jet charge, measured in the opposite hemisphere, depends directly on the mixing.

The $B^0\bar{B}^0$ mixing is now well measured [13]. Following the approach developed in the LEP oscillation working group [14], the simulation was tuned to reproduce the measured B fractions ($f_{B^\pm}$, $f_{B^0_d}$, $f_{B^0_s}$,$f_{B_{\rm baryon}}$) and the time dependence of the oscillations (Δm_d and Δm_s). The values and the corresponding uncertainties used to implement the $B^0\bar{B}^0$ mixing in the simulation are listed in Table 7.[11]

With this approach, the values estimated from the tuned simulation of $f^i_{b_r}$ and $f^i_{b_w}$ included the expected amount of mixing.

6.4 Results

The measured asymmetries and the corresponding statistical errors using the 1993–1995 lepton samples are listed below:

[10] The uncertainty due to the exact knowledge of these asymmetries is negligible compared with the error on the charge correlation itself.

[11] The values used come from the LEP Lifetime Working group (lifetimes), the LEP oscillation working group (fractions, Δm_d and Δm_s) and the LEP Heavy Flavour working group (χ). The lower bound value quoted for Δm_s was used ($\Delta m_s > 10.6\ ps^{-1}$), no sensitivity to the exact value of this parameter in the allowed domain has been observed. All these numbers are taken from [13].

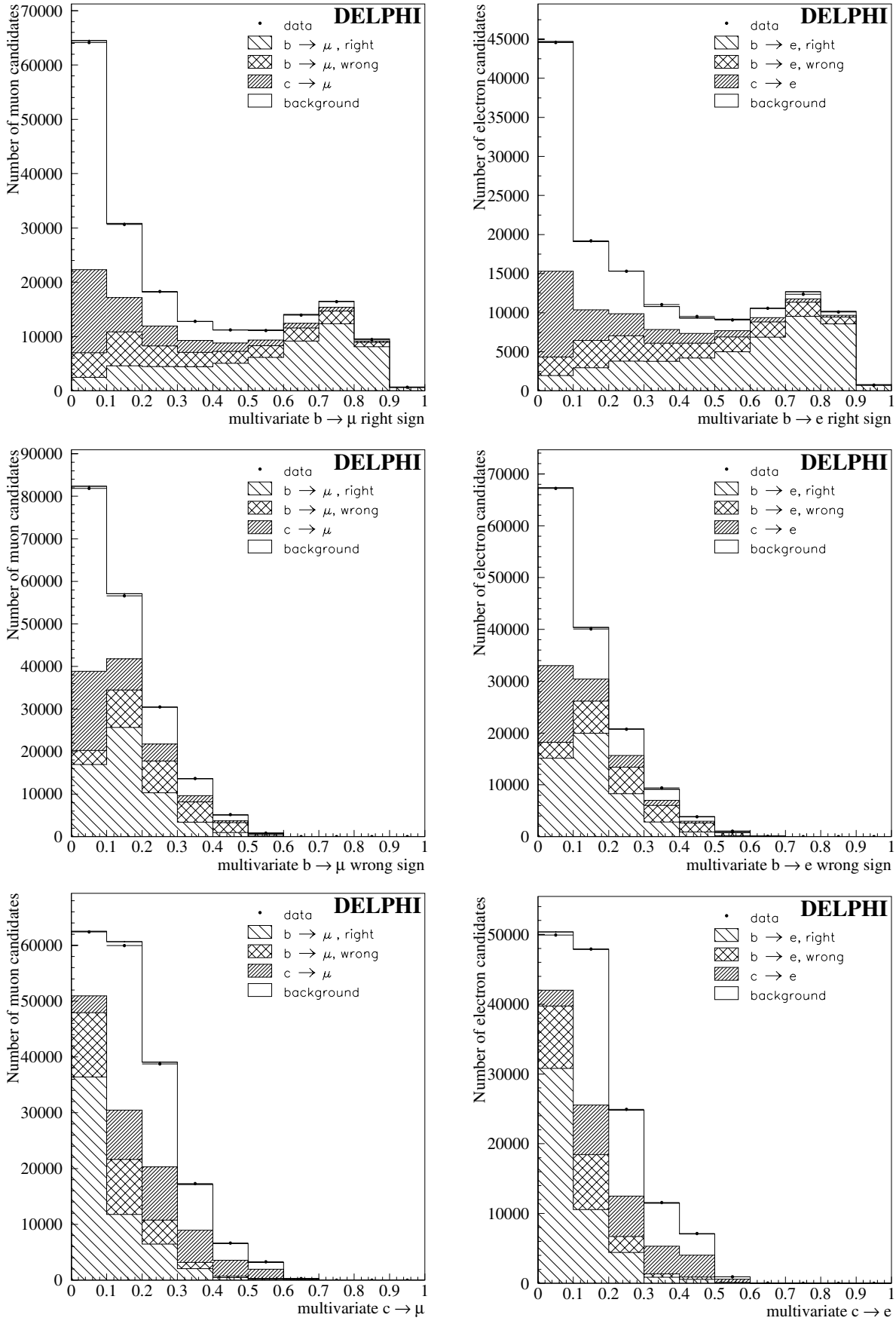

Fig. 3. Likelihood ratio $\mathcal{P}_{b_r}$ (up), $\mathcal{P}_{b_w}$ (middle) and $\mathcal{P}_c$ (bottom) distributions for muons (left) and electrons (right) for all years

Table 7. Different systematics in the χ^2 fit of the 1993–1995 DELPHI lepton sample at $\sqrt{s} = 91.22\,\mathrm{GeV}$. The systematic errors at $\sqrt{s} = 89.43\,\mathrm{GeV}$ were estimated to be $\pm\ 0.0024$ for $A_{\mathrm{FB}}^{\mathrm{b\bar{b}}}$ and $\pm\ 0.0046$ for $A_{\mathrm{FB}}^{\mathrm{c\bar{c}}}$, and at $\sqrt{s} = 92.99\,\mathrm{GeV}$ the corresponding values were $\pm\ 0.0024$ and $\pm\ 0.0070$

Parameters	Central value	Variations applied	$\Delta\ A_{\mathrm{FB}}^{\mathrm{b\bar{b}}}$ Peak	$\Delta\ A_{\mathrm{FB}}^{\mathrm{c\bar{c}}}$ Peak
$Br(b \to l)$	0.1056	$\pm$ 0.0026	$\mp$ 0.00048	$\pm$ 0.00062
$Br(b \to c \to l)$	0.0807	$\pm$ 0.0034	$\mp$ 0.00015	$\mp$ 0.00080
$Br(b \to \bar{c} \to l)$	0.0162	$^{+0.0044}_{-0.0036}$	$\pm$ 0.00017	$\pm$ 0.00180
$Br(b \to \tau \to l)$	0.00419	$\pm$ 0.00055	$\mp$ 0.00001	$\pm$ 0.00027
$Br(b \to J/\psi \to l)$	0.00072	$\pm$ 0.00006	$\pm$ 0.00005	$\pm$ 0.00002
$Br(c \to l)$	0.0990	$\pm$ 0.0037	$\pm$ 0.00036	$\mp$ 0.00182
$\Gamma_{b\bar{b}}/\Gamma_{\mathrm{had}}$	0.21644	$\pm$ 0.00075	$\mp$ 0.00007	$\pm$ 0.00007
$\Gamma_{c\bar{c}}/\Gamma_{\mathrm{had}}$	0.1671	$\pm$ 0.0048	$\pm$ 0.00034	$\mp$ 0.00130
$g \to b\bar{b}$	0.00254	$\pm$ 0.00051	$\pm$ 0.00012	$\pm$ 0.00005
$g \to c\bar{c}$	0.0296	$\pm$ 0.0038	$\pm$ 0.00012	$\pm$ 0.00001
$\langle X_E \rangle_B$	0.702	$\pm$ 0.008	$\mp$ 0.00016	$\mp$ 0.00019
$\langle X_E \rangle_{D^*}$ in $c\bar{c}$ events	0.510	$\pm$ 0.0094	$\pm$ 0.00047	$\mp$ 0.00046
b decay model [15]	$ACCMM$	$^{ISGW}_{ISGW**}$	$\mp$ 0.00065	$\mp$ 0.00111
c decay model [15]	$CL1$	$^{CL2}_{CL3}$	$\pm$ 0.00098	$\mp$ 0.00116
Total : Lepton Sample			$\pm$ **0.0015**	$\pm$ **0.0035**
$\tau_{B_d^0}$	1.548 ps	$\pm$ 0.032	$\pm$ 0.00005	$\pm$ 0.00004
$\tau_{B^\pm}$	1.653 ps	$\pm$ 0.028	$\mp$ 0.00002	$\mp$ 0.00003
$\tau_{B_s^0}$	1.493 ps	$\pm$ 0.062	$\mp$ 0.00025	$\pm$ 0.00001
$\tau_{B_{\mathrm{baryon}}}$	1.208 ps	$\pm$ 0.051	$\pm$ 0.00004	$\mp$ 0.00002
$\langle \tau_{B_{\mathrm{hadron}}} \rangle$	1.564 ps	$\pm$ 0.014	$\pm$ 0.00005	$\pm$ 0.00000
$\tau_{B^\pm}/\tau_{B_d^0}$	1.062	$\pm$ 0.029	$\pm$ 0.00016	$\pm$ 0.00001
$f_{b-\mathrm{baryon}}$	0.115	$\pm$ 0.020	$\mp$ 0.00006	$\pm$ 0.00010
$f_{B_s^0}$	0.117	$\pm$ 0.030	$\pm$ 0.00051	$\pm$ 0.00001
Δm_d	0.472 ps^{-1}	$\pm$ 0.017	$\mp$ 0.00003	$\pm$ 0.00008
χ	0.1177	$\pm$ 0.0055	$\pm$ 0.00082	$\pm$ 0.00001
Total : Mixing			$\pm$ **0.0010**	$\pm$ **0.0001**
Misidentified e		see text	$\pm$ 0.00011	$\pm$ 0.00021
Converted gammas in e sample		$\pm$ 10 %	$\mp$ 0.00019	$\mp$ 0.00050
Misidentified μ		see text	$\pm$ 0.00025	$\pm$ 0.00085
μ from π,K decay		$\pm$ 15%	$\pm$ 0.00027	$\pm$ 0.00092
background asymmetry		$\pm$ 40 %	$\mp$ 0.00076	$\pm$ 0.00421
p_T reweight of background		see text	$\mp$ 0.00007	$\pm$ 0.00021
Energy flow correction		see text	$\mp$ 0.00009	$\mp$ 0.00020
Total : Lepton identification and p_T measurement			$\pm$ **0.0009**	$\pm$ **0.0044**
b-tag tuning		see text	$\mp$ 0.00009	$\pm$ 0.00028
Merging for $N_{\mathrm{int}} = 2$		see text	+ 0.00061	− 0.00082
Jet charge stat		see text	$\mp$ 0.00052	$\pm$ 0.00070
Jet charge BKG subtraction		see text	$\mp$ 0.00069	$\pm$ 0.00084
Total : b-tag and jet charge calibration			$\pm$ **0.0011**	$\pm$ **0.0014**
Total			$\pm$ **0.0023**	$\pm$ **0.0058**

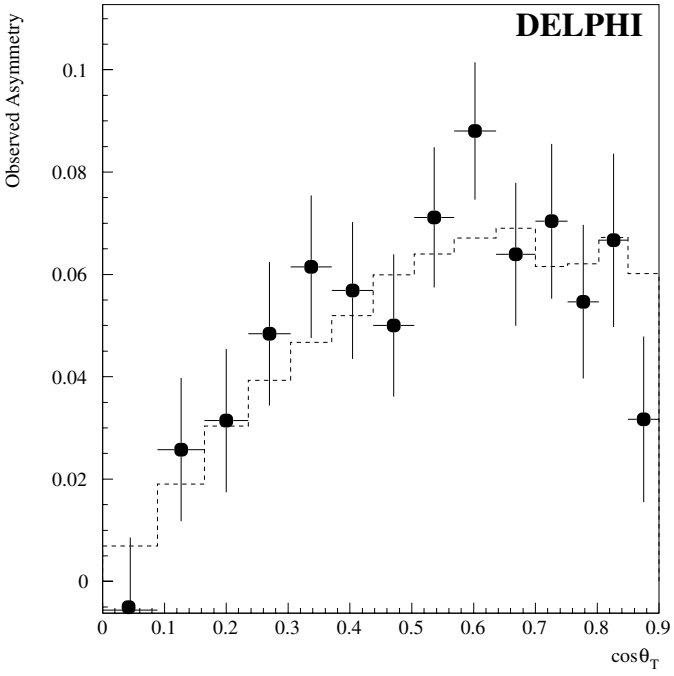

Fig. 4. Observed $A_{FB}^{\rm obs}$ asymmetry at peak energy as a function of $\cos\theta_T$ for a data subsample enriched in b with the right sign ($\mathcal{P}_{b_r} - \mathcal{P}_{b_w} > 0.6$). The result of the fit is shown as a dashed line

At $\sqrt{s} = 89.43\,\mathrm{GeV}$:

$$A_{\rm FB}^{b\bar{b}} = 0.066 \pm 0.022 \ \text{(stat)}$$

$$A_{\rm FB}^{c\bar{c}} = 0.030 \pm 0.035 \ \text{(stat)}$$

with a correlation of 0.19 and $\frac{\chi^2}{ndf} = \frac{185}{208}$, Prob($\chi^2$)=0.87;
at $\sqrt{s} = 91.22\,\mathrm{GeV}$:

$$A_{\rm FB}^{b\bar{b}} = 0.0958 \pm 0.0061 \ \text{(stat)}$$

$$A_{\rm FB}^{c\bar{c}} = 0.0585 \pm 0.0098 \ \text{(stat)}$$

with a correlation of 0.22 and $\frac{\chi^2}{ndf} = \frac{1416}{1453}$, Prob($\chi^2$)=0.75;
at $\sqrt{s} = 92.99\,\mathrm{GeV}$:

$$A_{\rm FB}^{b\bar{b}} = 0.109 \pm 0.018 \ \text{(stat)}$$

$$A_{\rm FB}^{c\bar{c}} = 0.108 \pm 0.028 \ \text{(stat)}$$

with a correlation of 0.19 and $\frac{\chi^2}{ndf} = \frac{204}{208}$, Prob($\chi^2$)=0.57.

The result of the fit for a data subsample is presented with the observed asymmetry in Fig. 4.

7 Systematic effects

The systematics from the different sources are listed in Table 7.

Lepton sample
To estimate the systematics due to uncertainties in decay branching ratios and spectra, the standard prescription of the LEP Heavy Flavour Working group was used [15]. The central values and variation were taken from [13] and [16] . The b and c decay model and their associated changes were taken from [15]. The variation considered for the lepton identification was described in Sect. 3.

Mixing
The combined effects of the uncertainties quoted in Table 7 for the parameters having a direct effect on the $B^0\bar{B}^0$ mixing description give a precision of $\pm$ 0.014 on $f_{B_s^0}$ and $\pm$ 0.005 on χ [13] following the method described in [14]. To take into account correctly the impact of the different sources of uncertainty on the $B^0\bar{B}^0$ mixing description, each of these measurements was varied within its error.

Background asymmetry
It should be noted that, while the observed "Background Asymmetry" systematic in $A_{\rm FB}^{c\bar{c}}$ comes from *uds* events, for $A_{\rm FB}^{b\bar{b}}$, the main source is the charge correlation between a fake lepton and the initial quark in b events themselves. Even if the charge correlation between the fake leptons and the initial quark of the corresponding event has been taken from the simulation, this correlation can be studied in the data using the $Q_\ell \times Q_{\rm opp}$ observable. Such charge correlation in b events is visible for example in the left plot of Fig. 2. In this case the $\sim$ 10 % of the difference in the amount of background between the two extreme $Q_\ell \times Q_{\rm opp}$ bins, originates from $b \to c \to s \to K^-$, where the $K^\pm$ is misidentified as a muon and behaves like a right sign lepton.

From these studies a conservative change of $\pm$20% in the charge correlation, corresponding to $\pm$40% variation in the background asymmetry, has been considered for the systematics. Such a change increases by 1.8 the χ^2 of the data/simulation comparison computed in the left plot of Fig. 2 corresponding to b-tag events enriched in fake leptons by a p,p_T cut. The same comparison done in the anti-b-tag bin (I), enriched in fake leptons from *uds* events, gives an increase of 1.3 in the χ^2.

The $A_{\rm FB}^{c\bar{c}}$ systematics are dominated by the contribution of the background asymmetry. This underlines the difficulty to separate the c events from the other flavours (see Fig. 3). The size of this systematic follows the variation of the asymmetries with $\sqrt{s}$ and explains most of the 50% increase in the $A_{\rm FB}^{c\bar{c}}$ systematics between $\sqrt{s} = 89.43\,\mathrm{GeV}$ and $\sqrt{s} = 92.99\,\mathrm{GeV}$.

Energy flow, p_T reconstruction
Due to a slightly worse energy reconstruction in the data, a 1–2 % shift in the jet energy distribution between data and simulation has been observed. This difference could have different effects on the asymmetries depending on its exact source (overall correction or sub-sample of charged/neutral track correction). The different possible sources were considered and the biggest effect observed was taken as the systematic error.
In the anti-b-tagged sample the shape of the p_T distribution of the lepton candidate was not correctly described by the simulation. This effect is known to be common to

all tracks from hadronisation in the tuned DELPHI simulation [8]. The full size of the correction estimated in the anti-b-tagged sample, was considered as a systematic error. It corresponds to changes $\sim \pm 5\%$ of the number of misidentified leptons as a function of p_T.

b-tagging

To take into account the effect of changes in the fraction r_q, defined in (5), the b-tagging corrections, $\delta_q^{(i)}$, were recomputed for each of the changes quoted in Table 7. For this reason all the quoted systematics also include possible variations induced by changes in the b-tagging tuning.

The systematic named *b-tag tuning* in Table 7, corresponds to the effects of the finite simulation statistics used to estimate the sample composition in the different b-tagged intervals and to the sensitivity to the correlation $\rho_q^{(i)}$ as described in Sect. 4.

The full difference between the results obtained for the two considered $N_{\rm int}$ choices (see Sect. 4) is quoted as *Merging for* $N_{\rm int} = 2$.

Jet charge

A jet charge tuning was performed for each computation of the systematics. For this reason, possible systematic errors in the jet charge tuning arising from the variation of a given parameter defined in Table 7 are included in the systematic errors of this parameter.

The systematic named *Jet charge stat* in Table 7, corresponds to the effect of the finite statistics used to estimate $\sigma_{Q_{{\rm jet},l}}$, f and $\overline{Q}_{{\rm jet},l}$. The systematic named *Jet charge BKG subtraction* in Table 7, is associated to the uncertainty on the jet charge description of non b events (see Sect. 5).

8 QCD corrections to the measured asymmetries

The QCD corrections applied to the asymmetries were obtained following the prescription given in [17]. This approach takes into account changes in these corrections due to experimental bias, like the suppression of events with an energetic gluon induced by the cut on the momentum of the selected leptons. The simulation sample, with an enlarged asymmetry [12] to improve the statistical precision of the study, was used to estimate such a bias. The relative change in the corrections due to experimental bias was estimated for this analysis to be 0.58 ± 0.08 for $A_{\rm FB}^{b\bar{b}}$ and 0.42 ± 0.12 for $A_{\rm FB}^{c\bar{c}}$. These scale factors were applied to the theoretical QCD corrections [13] and give the following QCD corrections : $A_{\rm FB}^{{\rm noQCD},x\bar{x}} = A_{\rm FB}^{x\bar{x}}/(1 - C_x)$ with $C_b = 0.0205 \pm 0.0046$ and $C_c = 0.0172 \pm 0.0057$.

[12] A value of 0.73 was used, slightly smaller than the maximal asymmetry allowed (0.75) to avoid the boundary problem and consequent asymmetric errors in the result of the fit

[13] $C_b^{{\rm had},T} = 0.0354 \pm 0.0063$ and $C_c^{{\rm had},T} = 0.0413 \pm 0.0063$ as recommended in [16].

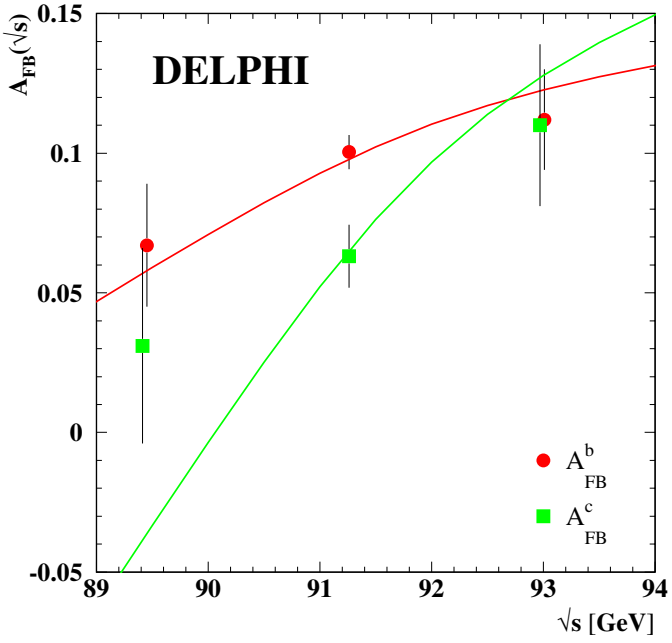

Fig. 5. Measured values of $A_{\rm FB}^{b\bar{b}}$ and $A_{\rm FB}^{c\bar{c}}$ at different $\sqrt{s}$ compared to the Standard Model predictions for $m_t = 175\,{\rm GeV}/c^2$ and $m_H = 300\,{\rm GeV}/c^2$ (To avoid the overlap of the results at peak-2 and peak+2, the $A_{\rm FB}^{b\bar{b}}$ and $A_{\rm FB}^{c\bar{c}}$ points have been shifted respectively by +0.02 GeV and -0.02 GeV.)

9 Conclusion

The heavy flavour asymmetry measurements presented in this paper, obtained with the 1993–1995 DELPHI data, can be combined with the 1991–1992 DELPHI measurements of $A_{\rm FB}^{b\bar{b}}$ and $A_{\rm FB}^{c\bar{c}}$ using leptons [3]. All asymmetry measurements were QCD corrected before averaging and the 1991–1992 DELPHI measurements were corrected to the same inputs (branching ratios and mixing) as the ones used in this paper.

Taking into account the correlations between the different systematic sources, the combined results are:

$$
\begin{aligned}
A_{\rm FB}^{b\bar{b}} &= 0.067 \pm 0.022 \ ({\rm stat}) \pm 0.002 \ ({\rm syst}) \\
&\quad {\rm at}\ \sqrt{s} = 89.43\,{\rm GeV} \\
A_{\rm FB}^{b\bar{b}} &= 0.1004 \pm 0.0056 \ ({\rm stat}) \pm 0.0025 \ ({\rm syst}) \\
&\quad {\rm at}\ \sqrt{s} = 91.26\,{\rm GeV} \\
A_{\rm FB}^{b\bar{b}} &= 0.112 \pm 0.018 \ ({\rm stat}) \pm 0.002 \ ({\rm syst}) \\
&\quad {\rm at}\ \sqrt{s} = 92.99\,{\rm GeV} \\
A_{\rm FB}^{c\bar{c}} &= 0.031 \pm 0.035 \ ({\rm stat}) \pm 0.005 \ ({\rm syst}) \\
&\quad {\rm at}\ \sqrt{s} = 89.43\,{\rm GeV} \\
A_{\rm FB}^{c\bar{c}} &= 0.0631 \pm 0.0093 \ ({\rm stat}) \pm 0.0065 \ ({\rm syst}) \\
&\quad {\rm at}\ \sqrt{s} = 91.26\,{\rm GeV} \\
A_{\rm FB}^{c\bar{c}} &= 0.110 \pm 0.028 \ ({\rm stat}) \pm 0.007 \ ({\rm syst}) \\
&\quad {\rm at}\ \sqrt{s} = 92.99\,{\rm GeV}.
\end{aligned}
$$

Figure 5 shows the energy dependence of $A_{\rm FB}^{b\bar{b}}$ and $A_{\rm FB}^{c\bar{c}}$ compared to the Standard Model prediction.

Following the general procedure described in [15], these results have been corrected to the Z pole; the energy shift from $\sqrt{s}$ to m_Z (for $\sqrt{s} = 89.43\,\mathrm{GeV}$: +0.0391, +0.0997; for $\sqrt{s} = 91.26\,\mathrm{GeV}$: −0.0013,−0.0034 ; for $\sqrt{s} = 92.99\,\mathrm{GeV}$: −0.0260, −0.0664), the effects of the initial state radiation (+0.0041,+0.0104) and γ exchange and $\gamma/\ Z$ interference (−0.0003,−0.0008) have been corrected by adding the quoted numbers respectively to $A_{\mathrm{FB}}^{\mathrm{b\bar{b}}}$ and $A_{\mathrm{FB}}^{\mathrm{c\bar{c}}}$. The averages of the pole asymmetries obtained after these corrections are :

$$A_{\mathrm{FB}}^{0,\mathrm{b}} = 0.1021 \pm 0.0052\ (\mathrm{stat}) \pm 0.0024\ (\mathrm{syst})$$
$$A_{\mathrm{FB}}^{0,\mathrm{c}} = 0.0728 \pm 0.0086\ (\mathrm{stat}) \pm 0.0063\ (\mathrm{syst})$$

in agreement with other DELPHI and LEP measurements [2, 18, 19].

The total correlation between $A_{\mathrm{FB}}^{0,\mathrm{b}}$ and $A_{\mathrm{FB}}^{0,\mathrm{c}}$ is +7%, with a correlation of +22% and -36% for the statistical and systematic errors respectively.

The effective value of the weak mixing angle derived from these measurements is

$$\sin^2\theta_{\mathrm{W,eff}}^{\mathrm{lept}} = 0.23170 \pm 0.00097.$$

Acknowledgements. We are greatly indebted to our technical collaborators, to the members of the CERN-SL Division for the excellent performance of the LEP collider, and to the funding agencies for their support in building and operating the DELPHI detector. We acknowledge in particular the support of Austrian Federal Ministry of Education, Science and Culture, GZ 616.364/2-III/2a/98, FNRS–FWO, Flanders Institute to encourage scientific and technological research in the industry (IWT), Federal Office for Scientific, Technical and Cultural affairs (OSTC), Belgium, FINEP, CNPq, CAPES, FUJB and FAPERJ, Brazil, Czech Ministry of Industry and Trade, GA CR 202/99/1362, Commission of the European Communities (DG XII), Direction des Sciences de la Matière, CEA, France, Bundesministerium für Bildung, Wissenschaft, Forschung und Technologie, Germany, General Secretariat for Research and Technology, Greece, National Science Foundation (NWO) and Foundation for Research on Matter (FOM), The Netherlands, Norwegian Research Council, State Committee for Scientific Research, Poland, SPUB-M/CERN/PO3/DZ296/2000, SPUB-M/CERN/PO3/DZ297/2000 and 2P03B 104 19 and 2P03B 69 23(2002–2004) JNICT-Junta Nacional de Investigação Científica e Tecnológica, Portugal, Vedecka grantova agentura MS SR, Slovakia, Nr. 95/5195/134, Ministry of Science and Technology of the Republic of Slovenia, CICYT, Spain, AEN99-0950 and AEN99-0761, The Swedish Natural Science Research Council, Particle Physics and Astronomy Research Council, UK, Department of Energy, USA, DE-FG02-01ER41155, EEC RTN contract HPRN-CT-00292-2002.

References

1. D. Bardin et al., Z. Phys. C **44**, 493 (1989); Comp. Phys. Comm. **59**, 303 (1990); Nucl. Phys. B **351**, 1 (1991); Phys. Lett. B **255**, 290 (1991) and Comp. Phys. Comm. **133**, 229 (2001)
2. DELPHI Collaboration, P. Abreu et al., Phys. Lett. B **276**, 536 (1992)
3. DELPHI Collaboration, P. Abreu et al., Z. Phys. C **65**, 569 (1995)
4. DELPHI Collaboration, P. Aarnio et al., Nucl. Instr. and Meth. A **303**, 233 (1991); DELPHI Collaboration, P. Abreu et al., Nucl. Instr. and Meth. A **378**, 57 (1996)
5. N. Bingefors et al., Nucl. Instr. and Meth. A **328**, 447 (1993)
6. V. Chabaud et al., Nucl. Instr. and Meth. A **368**, 314 (1996)
7. T. Sjöstrand, Comp. Phys. Comm. **82**, 74 (1994)
8. DELPHI Collaboration P. Abreu et al., Z. Phys. C **73**, 11 (1996)
9. JADE Collaboration, W. Bartel et al., Z. Phys. C **33**, 23 (1986); JADE Collaboration, S. Bethke et al., Phys. Lett. B **213**, 235 (1988)
10. DELPHI Collaboration, P. Abreu et al., Eur. Phys. J. C **20**, 455 (2001)
11. DELPHI Collaboration, P. Abreu et al., Eur. Phys. J. C **10**, 415 (1999)
12. DELPHI Collaboration, P. Abreu et al., Eur. Phys. J. C **9**, 367 (1999)
13. The Particle Data Group, D.E.Groom et al., Eur. Phys. J. C **15**, 1 (2000)
14. The ALEPH, CDF, DELPHI, L3, OPAL and SLD Collaborations (D. Abbaneo et al.), Combined results on b-hadron production rates and decay properties, CERN EP/2001-050
15. The LEP Experiments: ALEPH, DELPHI, L3 and OPAL, Nucl. Instr. and Meth. A **378**, 101 (1996)
16. The LEP/SLD Heavy Flavour Group, D. Abbaneo et al., Final Input Parameters for the LEP/SLD Electroweak Heavy Flavour analyses, LEPHF/2001-01, http://www.cern.ch/LEPEWWG/heavy/lephf0101.ps.gz
17. LEP Heavy Flavour Working Group, D. Abbaneo et al., Eur. Phys. J. C **4**, 185 (1998)
18. ALEPH Collaboration, R. Barate et al., Phys. Lett. B **434**, 415 (1998); ALEPH Collaboration, A. Heister et al., Eur. Phys. J. C **22**, 201 (2001); Eur. Phys. J. C **24**, 177 (2002); DELPHI Collaboration, P. Abreu et al., Eur. Phys. J. C **10**, 219 (1999); Eur. Phys. J. C **9**, 367 (1999); L3 Collaboration, O. Adriani et al., Phys. Lett. B **292**, 454 (1992); L3 Collaboration, O. Acciarri et al., Phys. Lett. B **439**, 225 (1998); Phys. Lett. B **448**, 152 (1999); OPAL Collaboration, G. Alexander et al., Z. fur Physik C **73**, 379 (1997); OPAL Collaboration, G. Abbiendi et al., Phys. Lett. B **546**, 29 (2002); Phys. Letts. B **577**, 18 (2003)
19. The LEP collaborations, the LEP electroweak working group and the SLD heavy flavour working group, A Combination of Preliminary Electroweak Measurements and Constraints on the Standard Model, CERN EP/2002-091, hep-ex/0212036